DEUTSCHES ELEKTRONEN – SYNCHROTRON

DESY 92-140
October 1992

First Results from the H1 Experiment at HERA

F. Eisele

Deutsches Elektronen-Synchrotron DESY, Hamburg

The H1 Detector at HERA

F. W. Brasse

Deutsches Elektronen-Synchrotron DESY, Hamburg

ISSN 0418-9833

NOTKESTRASSE 85 · D-2000 HAMBURG 52

To be sure that your preprints are promptly included in the
HIGH ENERGY PHYSICS INDEX,
send them to (if possible by air mail):

DESY **Bibliothek** **Notkestraße 85** **W-2000 Hamburg 52** **Germany**	**DESY-IfH** **Bibliothek** **Platanenallee 6** **O-1615 Zeuthen** **Germany**

DESY 92-140
October 1992

ISSN 0418-9833

First Results from the H1 Experiment at HERA

by F. Eisele *)
DESY

and

The H1 Detector at HERA

by F.W. Brasse *)
DESY

*) Talks at the XXVI International Conference on High Energy Physics at Dallas, 1992

FIRST RESULTS FROM THE H1 EXPERIMENT AT HERA

Franz Eisele
DESY
H1 collaboration:
RWTH Aachen, Univ. Antwerpen, Univ. Birmingham,
Univ. Libre und Vrije Univ. Brüssel, Rutherford Appleton Lab. Chilton,
Inst. Nucl. Phys. Cracow, Univ. of California Davis, Univ. Dortmund,
Univ. Glasgow, DESY und Univ. Hamburg, Univ. Kiel,
Inst. Exp. Phys. Kosice, Univ. Lancaster, Univ. Liverpool, QMWC London,
Univ. Lund, Univ. Manchester, ITEP und P.N. Lebedev Inst. Moscow,
MPI München, LAL Orsay, Ec. Polytechn. Palaiseau, P. & M. Curie Univ. Paris,
Univ. und Phys. Inst. der Akademie Prag, Univ. und INFN Rom, CEN Saclay,
Univ. GHS Wuppertal, IfH Zeuthen-DESY, ETH and Univ. Zürich.

Abstract

We report on the first physics studies with the H1 detector at the e-p collider HERA based on data with an integrated luminosity of $\int Ldt = 1.5\ nb^{-1}$ which were recorded in July 1992. The total γp cross section was measured at an average center of mass energy of $E^{\gamma p}_{CM} = 200$ GeV as $\sigma^{tot}_{\gamma p} = (150 \pm 26)\mu b$ (preliminary). The analysis of the hadronic final states in the quasireal interactions of photons with protons shows clear evidence for hard scattering processes both in single particle spectra and jet formation and good indications for the dominance of resolved photon contributions as predicted by QCD. HERA allows the investigation of deep inelastic scattering down to values of $x = 10^{-4}$ for $Q^2 > 5GeV/c^2$; two orders of magnitude lower in x than present fixed target experiments. The distributions of the first 200 events which were observed and identified in H1 are in good agreement with expectations . First limits on leptoquarks are presented.

INTRODUCTION

The events analysed in this paper were collected in July 29, 1992 during the first data taking period of the H1 detector at HERA. This accellerator collided beams of 26.7 GeV electrons with 820 GeV protons at about 2 permille of the design luminosity in a mode where 10 electron bunches collided with 10 proton bunches.

The runs selected for the present analysis had to pass stringent selection criteria on detector performance. They correspond to an integrated luminosity of 1.5 nb^{-1} for deep inelastic scattering and search for exotics and 1 nb^{-1} for the study of γp interactions .

THE H1 DETECTOR

A schematic view of the H1 detector is shown in Figure 1. It is asymmetric along

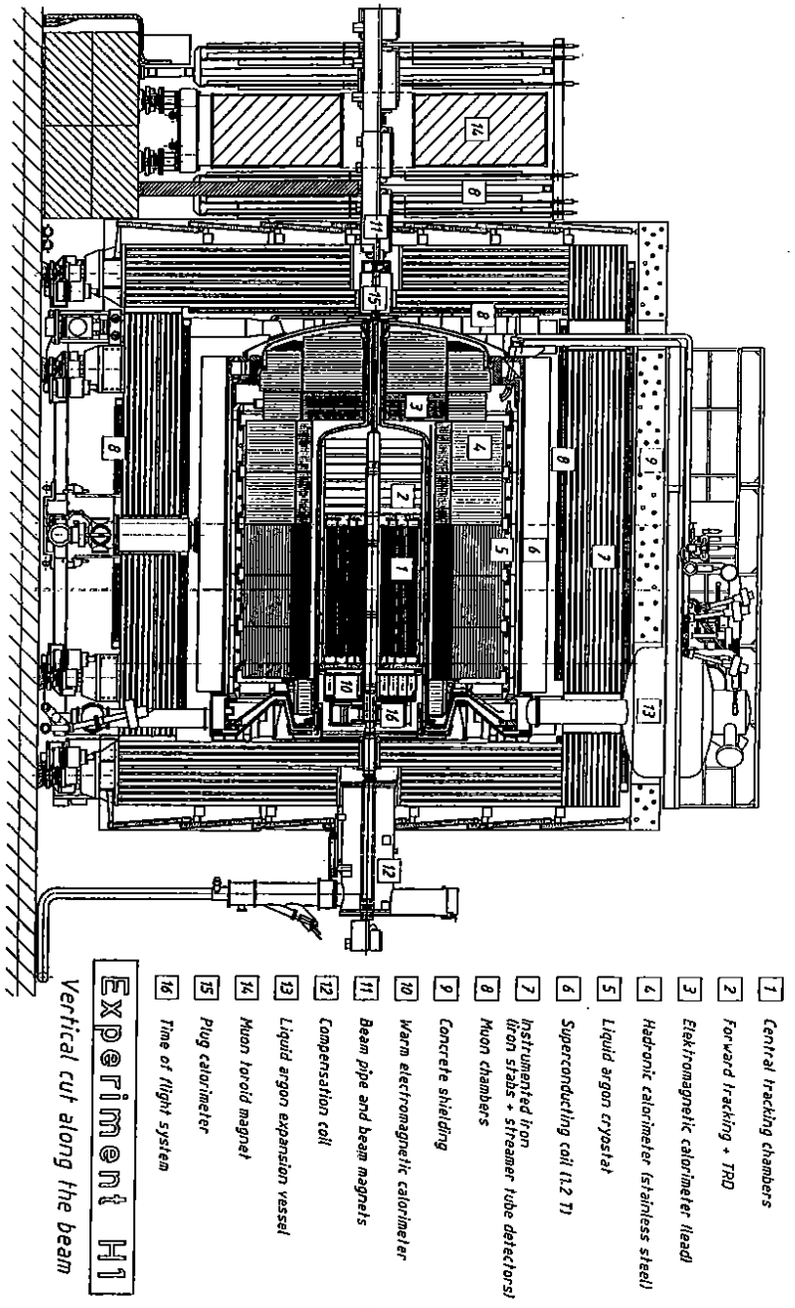

Figure 1. Schematic view of the H1 detector

the beamline since the high energy events are boosted in the proton (forward) direction leading to high particle energies and densities. The electron and proton bunches meet in an extended vertex region of about $\pm 50cm$. This region is surrounded by a system of cylindrical drift chambers for charged particle tracking: a jetchamber and 2 z-chambers. The forward tracking chambers consist of 3 radial and 3 planar drift chambers covering the angular range $7° < \Theta < 25°$. The backward region (electron direction) is covered by a multiwire proportional chamber with 4 wire planes which provides a space point up to angles of $\Theta = 175°$. Magnetic bending is provided by a superconducting solenoid at a radius of 3 m which produces a field of 1.2 T.

The tracking area is surrounded by a fine grain liquid argon calorimeter consisting of an electromagnetic section with lead absorber and a thickness varying between 20 and 30 radiation lengths , and a hadronic section with steel absorber and a thickness of 3.5 to 7 interaction lengths. The calorimeter stacks are housed in a single cryostat inside the coil. The backward region is covered by a warm lead scintillator electromagnetic calorimeter (BEMC). The iron yoke is instrumented with plastic limited streamer tubes and acts as muon detector and tail catcher calorimeter. Additional muon chamber planes are added inside and outside of the iron. Muon detection is supported further by a forward spectrometer consisting of an iron toroid and 6 layers of drift chambers. Small angle photon and electron tagging counters are placed 33m (electron tagger) and 100 m (photon tagger) upstream of the detector. They are used to measure the luminosity via the reaction $ep \rightarrow ep\gamma$ and to tag and trigger on electrons and photons.

A summary of important detector parameters is given in table 1.

Data selection and reduction

Triggering and fast data reduction is a big challenge at HERA even at 1 permille of design luminosity because electron and proton gas interactions and the interaction of halo particles near the detector can deposit much more energy into the detector than many interesting ep events and at much higher rates. The triggering and data reduction is therefore done in several levels as schematically illustrated in Figure 2. The first trigger level (L1) stops the pipeline after 25 bunch crossings (2.5 μs). The main trigger elements used at the moment are :

- a global VETO derived from a two plane time of flight scintillator hodoscope behind the BEMC to reject upstream proton interactions.
- electron triggers based on cluster energies in the BEMC , liquid argon calorimeter or the electron tagger
- triggers based on two cylindrical multiwire proportional chambers which cover the angular range $25 < \Theta < 155°$. Both 'ray triggers' and z-vertex (ZVRTX) triggers which ask for a significant peak in a vertex histogram are used.
- transverse and missing energy triggers using the liquid argon calorimeter
- muon triggers

The next level of data reduction is done on the filter farm (trigger level L4) which consists presently of 15 VME based RISC processors which perform fast filter algorithms and a partial reconstruction of events. At present full reconstruction of the tracks in the central

H1 Detector Parameters

CALORIMETRY	Main calorimeter Liquid Argon • Stability ≤ 0.2 % over 1 year • noise 10-30 MeV/channel • dead channels < 0.3 % 4° < Θ < 155°	EMC (Pb)	$\Delta E_e / E_e = 12\%/\sqrt{E_e} \oplus 1\%$	transverse 4*4 cm² longitudinal 3+ 4 segm channels 32000
		HAC (Steel)	$\Delta E_H / E_H < 50\%/\sqrt{E_H} \oplus 1\%$	transverse 8*8 cm² containment 4.7+8 λ_{abs} channels 13000
	Backward el.magn. Calorimeter (BEMC) 150°<Θ<174°	Pb/Sci	$\Delta E_e / E_e = 10\%/\sqrt{E_e} \oplus 1\%$	transverse 15*15 cm² 2 longitudinal segments
TRACKING	Coil (S.C.) r = 3 m	$B = 1.2T$ $\Delta B / B \leq 2\%$		
	Central Tracking 25°<Θ<155° $\Delta P/P^2 < 0.003$	jet chamber:	$11cm < r < 85cm$ 56 radial wires $\Delta(dE/dx) = 10\%$ $\sigma_{r\phi} \cong 160\mu m$ $\sigma_z \cong 2.5cm$	
	Forward Tracking 7°<Θ<25°	radial & planar chambers 72 wires along beam		

Table 1.

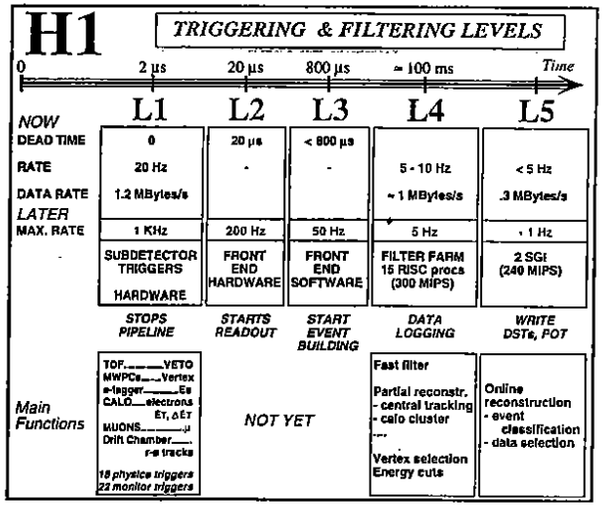

Figure 2.

jet chamber and a vertex fit is done. In addition we filter out cosmic muons and sharpen energy thresholds of the calorimeter triggers. The rejection factor is adjusted such that the accepted events are logged at the DESY mainframe with a maximum rate of about 5 Hz. All events are then reconstructed quasi online (with about 2 hours delay) on a Silicon Graphics RISC workstation with 6 processors. At the same time an event classification is carried out which is the basis to write the selected events to the production output tapes (cartridges) and to the data summary tapes (fast disk pool).The DST contains all events which are regarded to be of interest for the physics analysis. This scheme allows to get fast access to the interesting data with a very small time delay.

Status of detector

The detector is nearly complete with exception of a fraction of the muon instrumentation (20%) and about 30% of missing FADC's in the forward tracker. Finally significant improvements in the trigger area are under way. The H1 detector and its physics potential is described in more detail in the contribution of F. Brasse to this conference[1].

DEEP INELASTIC SCATTERING

The kinematic range of HERA extends up to values of $Q^2 \sim 5 * 10^4\ GeV^2$ both for neutral and charged current scattering, 2 orders of magnitude larger than fixed target experiments.

At low luminosity however we expect only neutral current events at low Q^2 but up to large energy transfer. Most of the scattered electrons of these events are detected in the backward electromagnetic calorimeter (BEMC) and only a small fraction is seen in the liquid argon calorimeter. The event selection poses the following requirements:

- at the hardware trigger level (L1): cluster energy in the BEMC E_{clu}^{trig} >4 GeV and no time of flight veto from the upstream TOF scintillator hodoscope
- at the reconstruction level (L4/L5): reconstructed cluster energy in the range $6 < E_{clu} < 32\ GeV$, for $6 < E_{clus} <$22 GeV in addition a good vertex and the matching of a track or a BPC hit with the cluster within 15 cm radius.

A low Q^2 event is shown in Figure 3. The data reduction is graphically illustrated in Figure 4 , the background level has to be reduced by about 4 orders of magnitude to get to the e-p interaction events.

Comparisons with Monte Carlo predictions

The cluster energy spectrum of the selected events is shown in Figure 5 compared to MC expectations. Detailed crosschecks and visual scanning of all events demonstrate that these events are genuine e-p events in the vertex region. The region at low cluster energies is however strongly contaminated by photoproduction events where pions are misidentified as electrons. This interpretation is supported by the fact that a large fraction of these events has a tagged electron in the electron tagger. This photoproduction background can be eliminated by using the e/π separation potential of the BEMC and by kinematic selection but no final results can be presented yet.

In the following comparisons with DIS MC's will be restricted to the 141 events with cluster energy above 12 GeV which are deep inelastic events with very little background. The MC predictions are based on

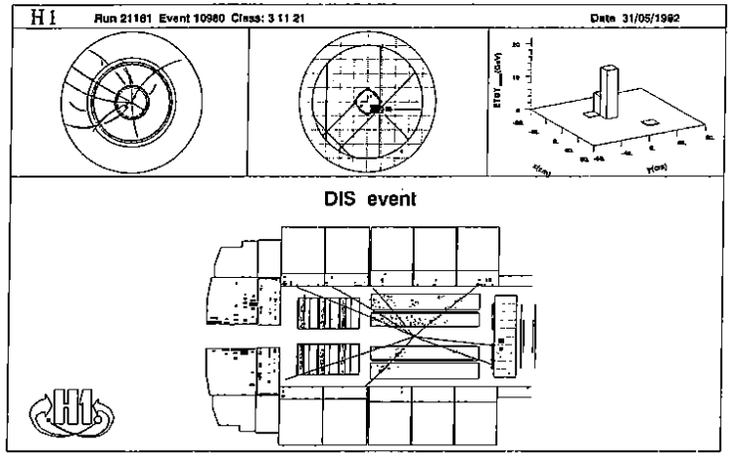

Figure 3. Low Q^2 deep inelastic event as seen in the H1 detector

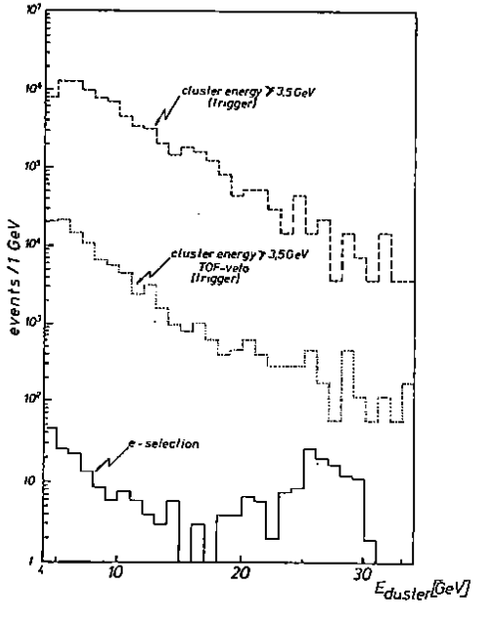

Figure 4. Event rates for low Q^2 deep inelastic events vs. cluster energy at different levels of data selection

the DJANGO[2] generator which includes radiative corrections and initial state QCD radiation. Two predictions with different sets of structure functions are shown: one with a 'flat' gluon distribution and one with a 'steep' gluon distribution. The prediction is absolutely normalised to the integrated luminosity. The following conclusions can be drawn: 1) The calorimeter is decently calibrated since it reproduces the position of the 'kinematic peak' at the beam energy to about 3% accuracy. With increasing statistics this peak will be used later to actually determine and monitor the calibration accurately. 2) The data are reasonably well described by MC in shape and magnitude within our 10% normalisation uncertainty. 3) Within the limited statistics and in the reduced kinematic range the data are not yet able to distinguish between different structure function sets.

The distributions in x and Q^2 are shown in Figure 6 for $.05 < y < .55$ ($E_e > 12$GeV) where these variables are well measured with the electron alone. Again the agreement in

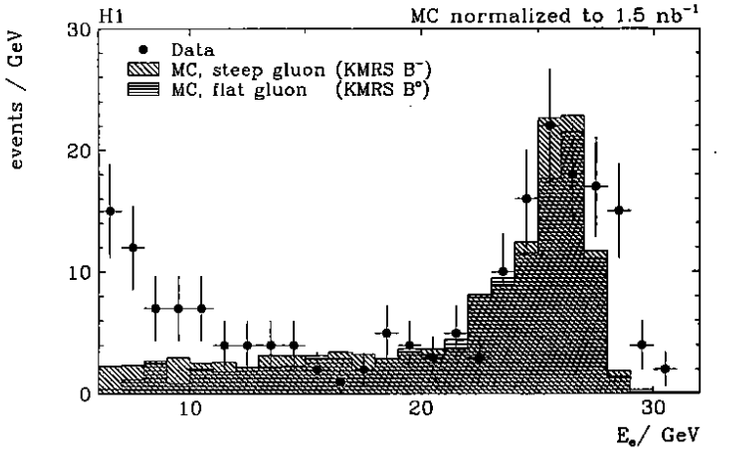

Figure 5. Energy spectrum of the 'electron' cluster for deep inelastic event candidates compared to MC predictions for two sets of structure functions. The MC predictions are absolutely normalised with an uncertainty of 10%

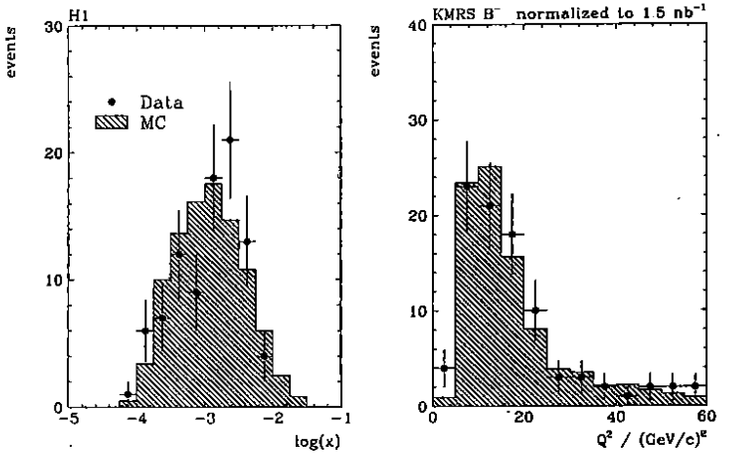

Figure 6. Distributions in x and Q^2 for the events in the range $.05 \leq y \leq .55$ compared to an absolutely normalised MC prediction.

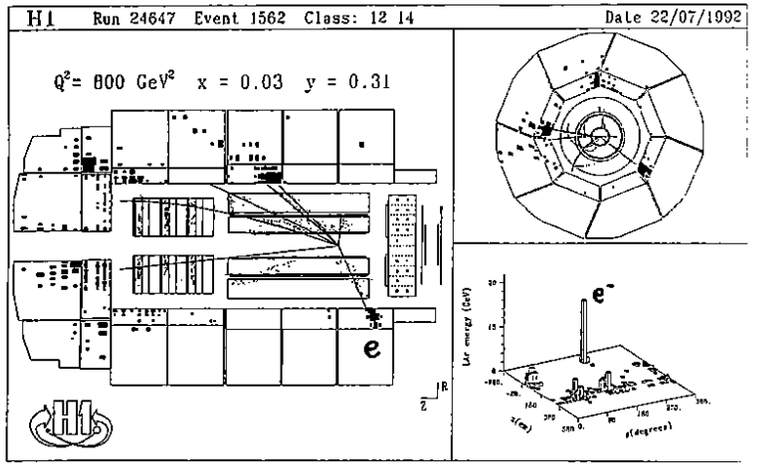

Figure 7. High Q^2 deep inelastic event in the H1 detector

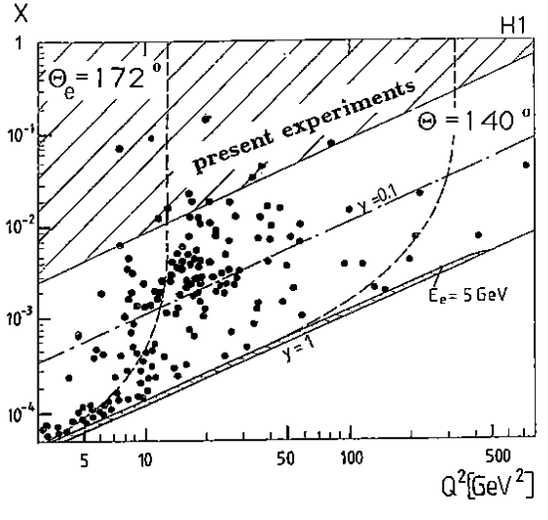

Figure 8. The position of all DIS events in the (x, Q^2) plane compared to the area accessible to fixed target experiments so far

shape and magnitude is good.

We have also found 5 higher Q^2 events where the electron is recorded in the liquid argon calorimeter. The event with highest $Q^2 \sim 800\ GeV^2$ is shown in Figure 7. All events are shown in the (x, Q^2)-plane in Figure 8 together with the area which was accessible in fixed target experiments so far. HERA extends the range down to values of $x=10^{-4}$ by two orders of magnitude.

This is important and interesting for two reasons: 1)The low x structure functions are needed as phenomenological input for the prediction and interpretation of physics at SSC and LHC in the same way as the new structure function measurements of the NMC collaboration are essential for the interpretation of the CDF results. There is no way how present measurements can be extrapolated ; we need a direct measurement which can only be done at HERA. 2) At these low values of x, the parton density has to become very large according to QCD. As a result the partons cannot behave freely , they must show recombination and eventually saturation effects. HERA offers a good chance to study this new regime of QCD especially if the partons are not uniformly distributed in the proton but clustered e.g. around the valence quarks (hot spots).

Hadronic final state in DIS

The hadronic final state can be studied based on the calorimeters alone or using charged tracking in combination with the calorimeters which improves the resolution at low energies. Figure 9 shows the transverse

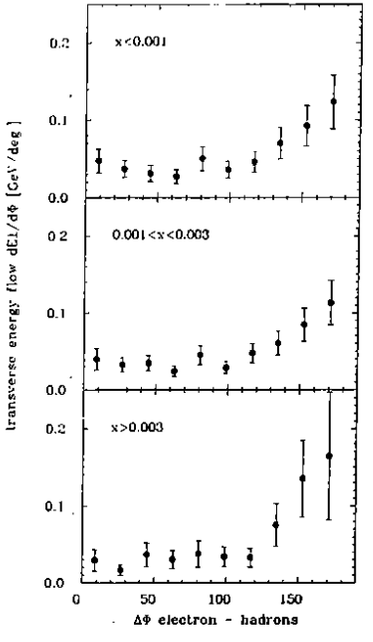

Figure 10. Transverse hadronic energy flow in Φ relative to the electron direction

momentum balance between the electron and the hadrons compared to MC predictions. Obviously the energy scales of electrons and hadrons match well and the resolutions are well described by our MC. Electrons and hadrons are back to back in ϕ as expected. The jet structure of the final state is demonstrated in Figure 10 which shows the transverse hadronic energy flow with respect to the electron direction. With increasing x the hadrons are more and more collimated

opposite to the electron as expected.

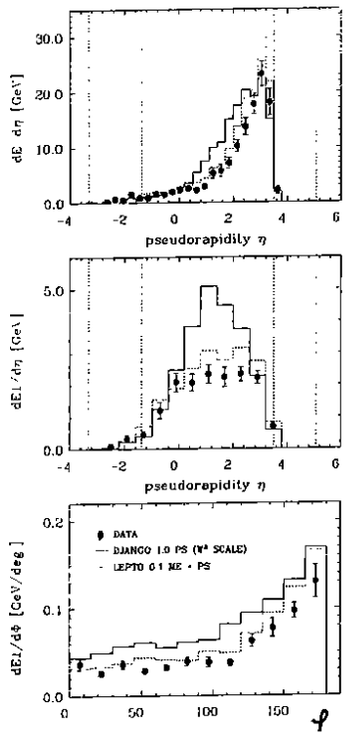

Figure 11. Hadronic energy flow as measured in the calorimeter. a) energy vs. pseudorapidity b) transverse energy vs. pseudorapidity c) transverse energy relative to the electron direction compared to two MC predictions

Here we have selected events with $W^2 > 3000\ GeV^2$. Finally we show the hadronic energy flow in rapidity and φ compared to two different generator models (Figure 11). They show significant differences. It is clear that at HERA we need data to tune the MC's; we are just starting to do so.

SEARCH FOR EXOTICS

HERA is an ideal place to look for compositeness and this is most easily done by searching for composite particles like leptoquarks , excited electrons and others. Another interesting subject is the search for heavy fermions like a heavy Majorana neutrino. We have looked for exotic objects and found none. To illustrate the potential of HERA the present result for the leptoquark search is given in Figure 12 which shows the excluded regions in a plot of the coupling constant λ versus mass together with results from the $\bar{p}p$ collider experiments and low energy bounds. In addition the expected sensitivity for an integrated luminosity of 1 and 100 pb^{-1} at HERA is also shown. Though the present bounds are not yet very interesting, HERA will very fast get a chance to make sensitive searches and eventually find new physics.

PHOTOPRODUCTION

The interaction of quasireal photons with protons at HERA can be studied up to center of mass energies of $E^{\gamma p}_{CM}$ = 270 GeV corresponding to E^{γ}_{lab}= 39 TeV for fixed target experiments. The questions adressed in our first analysis are how large is the total cross section , do we have evidence for hard scattering processes, and can we confirm specific QCD predictio ns? Two data samples are used for this analysis:

- A tagged sample based on events where the electron was seen in the electron tagging detector under angles $\prec$ 5 mr in the energy range $6 \prec E_e \prec 19\ GeV$. The event selection asks for an electron tagging trigger with $E^{trig}_{tag} > 4\ GeV$ and

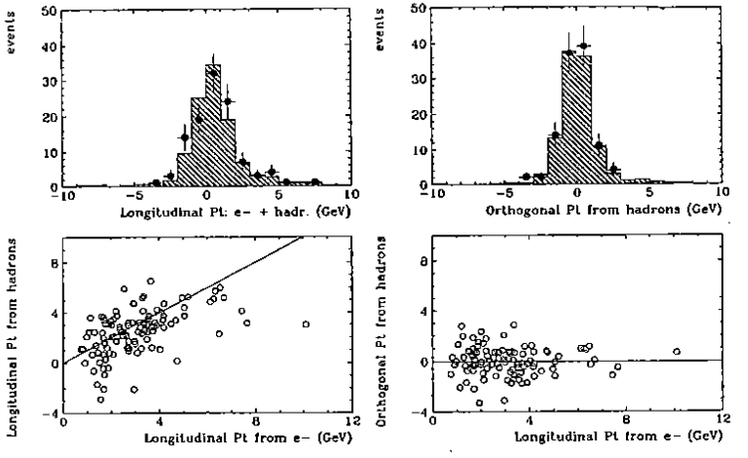

Figure 9. Transverse momentum balance between electron and hadrons in DIS

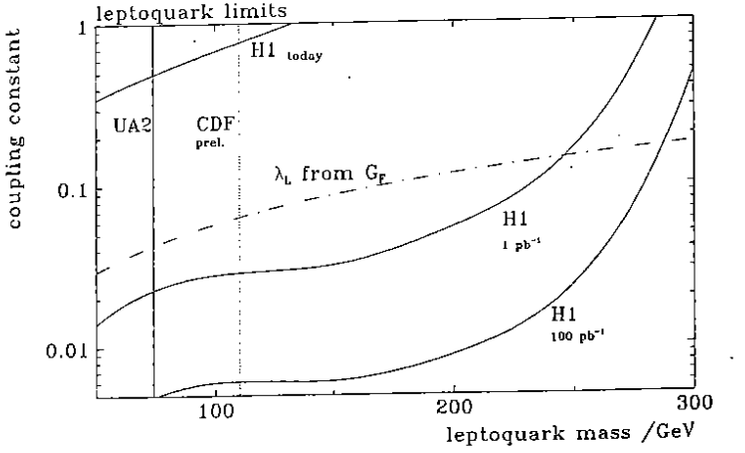

Figure 12. Limits on leptoquark production

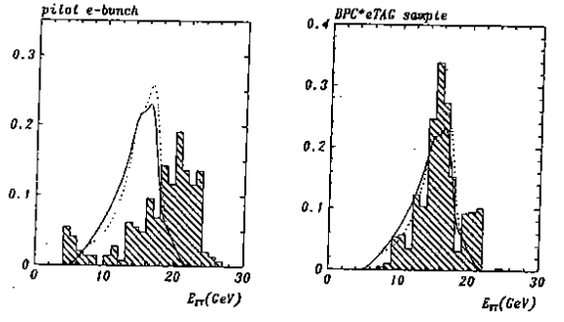

Figure 13. Energy spectrum of tagged electrons for background events from the electron pilot bunch (left) and for the tagged events compared to the tagger acceptance (curves)

one trigger ray in the central multiwire proportional chambers (A ray is equivalent to one charged track in the angular range $25^o < \Theta < 155^o$ with $p_T > .3\ GeV/c$). After reconstruction we ask in addition one good reconstructed central track pointing to the vertex region.

- a high E_T sample which is used for jet studies. These events are triggered by the ZVTRX trigger of the central multiwire proportional chambers. After reconstruction we ask for one good track to the interaction region and a transverse energy $E_T^{barr} > 10$ GeV for $\Theta > 25^o$ measured in the calorimeters.

Both event samples have large backgrounds due to proton- and electron-gas interactions in the vertex region.

Total cross section measurement

This measurement is based on the tagged data sample. The beam gas backgrounds are first reduced by asking in addition at least one reconstructed hit in the backward proportional chamber. The remaining background, mainly proton background with a random e-tag coincidence,is then statistically subtracted using the shape of the measured energy spectrum of the tagged electrons which is substantially different for background and signal as shown in Figure 13 . The background spectrum can be determined from the events produced by the 'electron pilot bunch' which is not colliding with a proton bunch. We are left with 602±61 events corresponding to a total integrated luminosity of $994\mu b^{-1}$. The luminosity is determined with an accuracy of 10%, the photon flux folded with the electron tagging acceptance is known to about 8%. The remaining problem is the determination of the acceptance of the events in the main H1 detector. Unfortunately this acceptance is very different for the different processes which contribute to the total cross section . They can be roughly classified as follows: i1) σ_D: elastic and diffractive contributions. ii) σ_{inel}: low E_T inelastic contributions which are modeled by RAYPHOTON[2] and contain no hard scattering contribution and finally iii) σ_{jet}: hard photon parton or parton parton scattering which we model by the jet generator PYTHIA 5.6[2] The cross section is then evaluated making assumptions on the composition of the total cross section:

$$\sigma_D : \sigma_{inel} = .28 : .72 \quad (model\ 1)$$

$$\sigma_D : \sigma_{inel} : \sigma_{jet} = .28 : .52 : .20 \quad (model\ 2)$$

The results are summarised in table 2.

Model 1 gives an upper limit to the cross section measurement since jet contributions have higher acceptance than the others. Any addition of a jet contribution will therefore lower the cross section. Our best guess for the jet contribution is obtained from our analysis of the hard scattering presented below and enters model 2 (see below). We have made similar evaluations of the cross section with different data selections and strongly varying acceptances which agree well with the main result giving us confidence that we understand our systematic effects. These results are not corrected for radiative effects. Our preliminary analysis gives a correction of about 2.5% which lowers σ_{tot}.

Our final result is:

$$\sigma_{tot}^{\gamma p} = (150 \pm 15_{stat} \pm 19_{syst})\mu b.$$

It is shown in Figure 14 together with measurements at low energy and several theoretical predictions.

It compares well with the simplest models which predict a rise similar to the proton proton cross section[3] and excludes large values as predicted by 'minijet' models[4].

Table 2. Determination of the total cross section

events	$L\ (\mu b^{-1})$	acceptance %					$\sigma_{tot}^{\gamma p}$	$\sigma_{tot}^{\gamma p}$
		ϵ_D	ϵ_{inel}	ϵ_{jet}	$\bar{\epsilon}(model\ 1)$	$\bar{\epsilon}(model\ 2)$	(model 1)	(model 2)
602±61	994±100	20	62	86	50.2±4.2	55.0±4.5	165 ± 28	150 ± 26

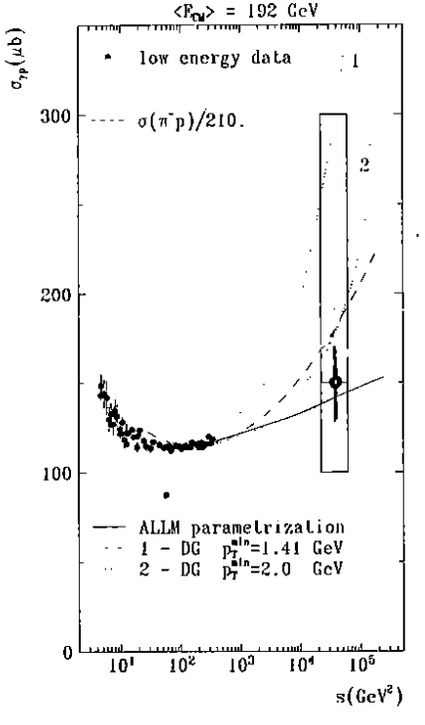

Figure 14. Measurements of the total photoproduction cross section from H1 and from low energy experiments compared to theoretical predictions

Evidence for hard scattering processes

Hard scattering processes are expected in VDM where partons inside the vector meson can scatter with partons in the proton and in QCD which predicts 'direct photon' processes and 'resolved photon' processes as illustrated in figure 15. All hard scattering processes are modeled in our analysis by the PYTHIA 5.6[2] generator.

The specific QCD prediction at HERA is that the resolved processes should dominate at low E_T over the direct processes in contrast to present fixed target experiments where direct photon processes dominate.

Single particle spectra

Charged single particle spectra were measured using the tagged sample. For this analysis the beam gas backgrounds were eliminated by kinematic cuts based on the correlation between $y_{tag} = E_\gamma/E_e$ and $y_{calo} = \sum_i(E_i - p_{z_i})/2E_e$ where the second quantity is measured summing over all calorimeter cells i. We require $y_{calo} > .2$ and $.35 < y_{tag} < .7$ which eliminates essentially all proton induced background. Remaining background from the electrons is eliminated by asking an energy deposit in the forward calorimeter $E_{fwd} > 5GeV$ within the cone $\Theta < 25^o$. The final sample after these cuts consists of 222 tagged electron events which contains $0 \pm 2\%$ beam gas background.

Figure 16 a) and b) shows the rapidity distribution for all central charged tracks

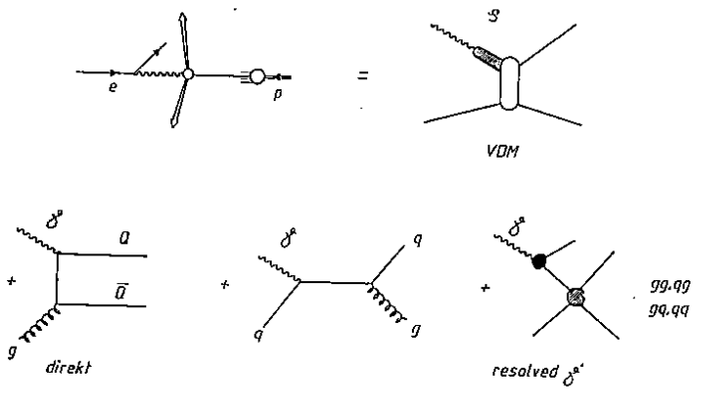

Figure 15. Basic photoproduction processes

and the P_T^2 distribution compared to the expectations of hard scattering processes modeled by the jet MC PYTHIA 5.6 and to low P_T processes modeled by the generator RAYPHOTON[2] which describes ρp interactions without the hard scattering contribution. The data exhibits a significant tail in P_T^2 which is naturally explained by the jet MC if we choose a cut $\hat{P}_{T,min} > 2.5\ GeV$. The variable $\hat{p}_{T,min}$ is a measure for the hardness of the process and a free parameter of the generator.

We conclude that we have evidence for the existence of hard scattering processes and that they are well described by our jet MC provided we choose a $\hat{p}_{T,MIN}$ of about 2.5 GeV.

Jets in γp

The existence of hard scattering processes must lead to the observation of jets at high E_T. The analysis is based on the high E_T sample of events. Energies are measured with the calorimeters only. Large transverse energies in the liquid argon calorimeter can sometimes be faked by an overlay of a halo muon traveling parallel to the liquid argon gaps and by bursts of coherent noise which occur sporadically. These events are eliminated by program and verified by visual inspection.

We use a cone jet algorithm where we ask for two or more jets with $E_T > 3$ GeV in a cone of radius $R = \sqrt{\Delta\eta^2 + \Delta\phi^2} = 1.0$ where η and ϕ are the rapidity and azimuthal angle of the jet axis respectively. The selected events still show a sizeable fraction of proton gas background events where both jets are going forward. This background is eliminated by asking for an opening angle between the two jets with highest E_T larger than 60°. Few remaining deep inelastic events are removed by kinematic cuts. We are left with 34 γp events with at most 8% background. This is confirmed by all control plots like average charge of charged particles, dE/dx measurements, vertex distribution etc. In the sample of 34 events we find 7 which have a tagged electron. In addition we have 7 more tagged events from the tagged sample which have not fired the ZVTRX trigger. One of the selected jet events is shown in Figure 17. Obviously we cannot expect spectacular jet signatures

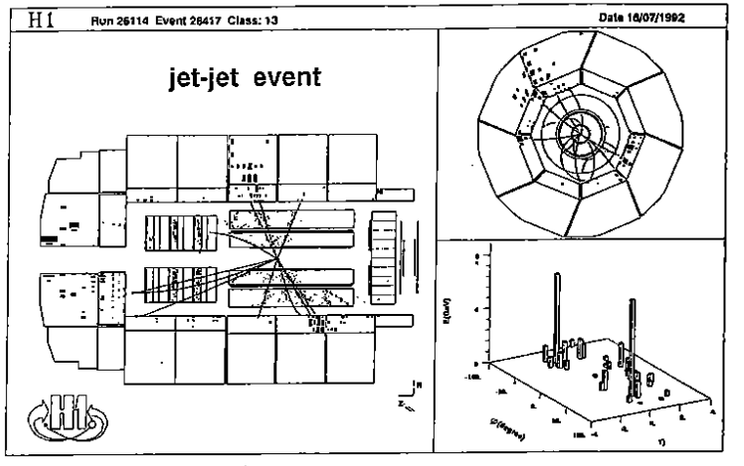

Figure 17. Two jet photoproduction event as seen in the H1 detector

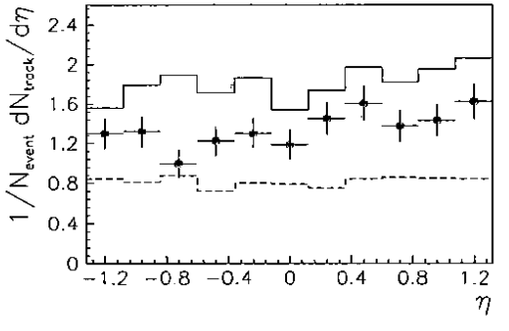

Figure 16a. Multiplicity of charged tracks per event with $p \geq .3$ GeV in the central region compared to the jet Monte Carlo (PYTHIA 5.6 with $\hat{p}_{T;min}$ = 2.5 GeV^2) and a low P_T MC (RAYPHOTON).

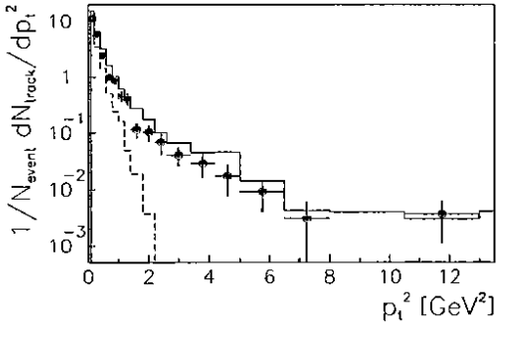

Figure 16b. P_T^2 distribution of charged tracks with $p \geq .3$ GeV in the central region compared to the jet Monte Carlo (PYTHIA 5.6 with $\hat{p}_{T;min}$ = 2.5 GeV^2) and a low P_T MC (RAYPHOTON).

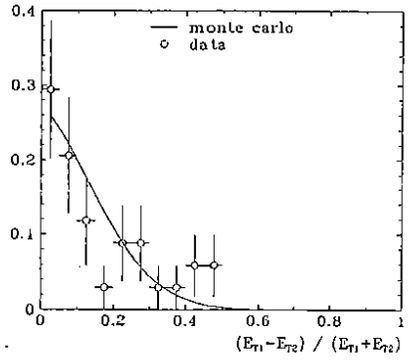

Figure 18a. Distribution of the E_T balance of the two jets with highest E_T compared to the MC expectation

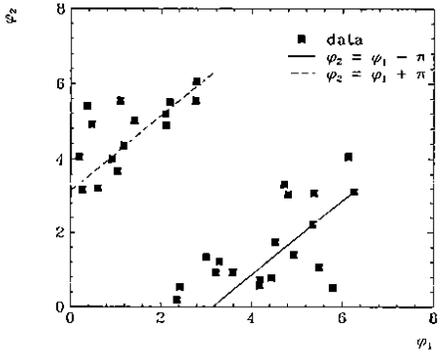

Figure 18b. Angular correlation of the two jets with highest E_T in the azimuthal plane

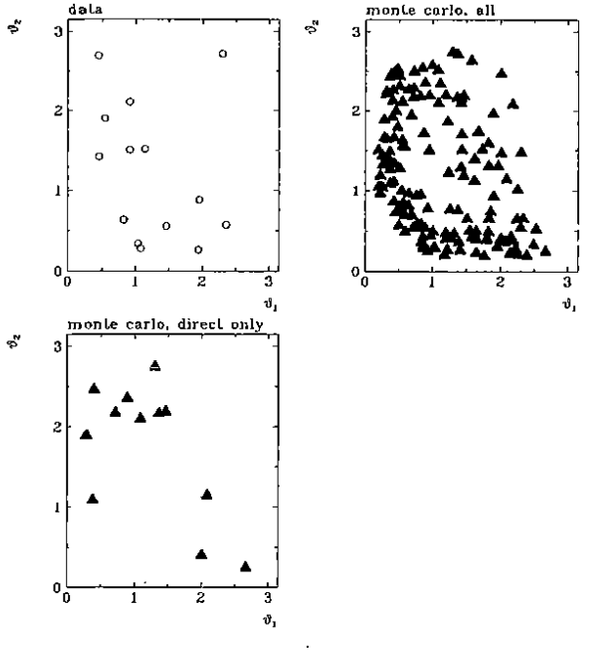

Figure 19. Correlation of the polar angles for the two jets with highest E_T
for events with an electron tag a) for 14 data events
b) for all events of the jet MC (dominated by resolved photon contributions)
c) MC prediction for direct photon processes only

for our low E_T events. We expect however that the two jets with largest E_T represent the two scattered partons and are therefore approximately balanced in E_T and back to back in ϕ. This is indeed the case (Figure 18 a) and b)) and the distributions are well described by the jet MC. More statistical tests were made so that we are convinced that we see jets in our data. Next we can check specific predictions. Figure 19 shows the the correlation between the polar angles of the two jets for the 14 events with tagged electron. In these events the energy of the incoming photon is known and thus the momentum vectors of the two outgoing jets are constrained in direct photon processes in contrast to resolved processes where only a fraction of the photon energy is transfered to the hard scattering. On the parton level this constraint is given by $2E_T/E_\gamma = tan\ \Theta_1/2 + tan\ \Theta_2/2$. The results of the jet MC for all processes (dominated by resolved photon processes) and for the direct processes only are also shown in Figure 19. The data are well compatible with the prediction of the jet MC but disagree with the assumption that only direct processes are observed. The jet cross section $dN/dE_T/GeV^{-1}$ is shown in Figure 20 together with predictions of the jet MC normalised to the same integrated luminosity.

The rates show good agreement within the estimated normalisation uncertainty of a factor 2 for a value of the parameter $\hat{p}_{T,min}$ of about 2.5 GeV. The factor 2 is the combined effect of the uncertainty in the structure functions, the error on the trigger acceptance and the calibration uncertainty of about 5%. For comparison we also show the absolute prediction for the direct photon processes only using $\hat{P}_{T,min} = 1GeV$ which is far below our data.

We therefore conclude that we have evi-

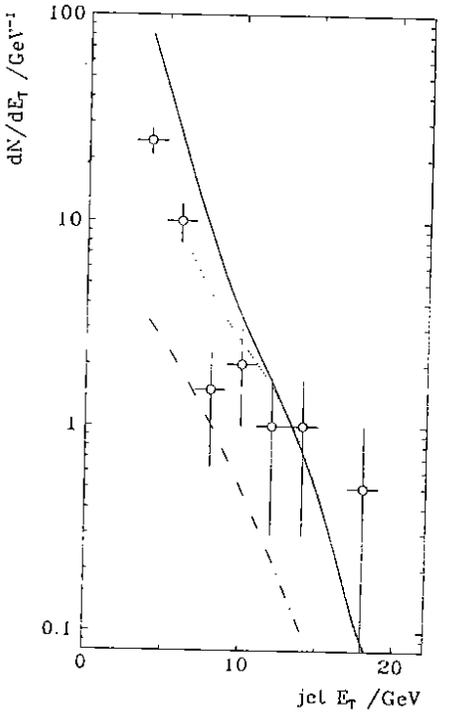

Figure 20. Inclusive p_T distribution of the jets. The lines are absolute predictions of the jet MC PYTHIA 5.6 for values of $\hat{p}_{T;min}$=1 GeV (solid curve) and 5 GeV (dotted curve). Also shown is the prediction for the direct photon processes only (dash-dotted line) for $\hat{p}_{T;min}$=1 GeV

dence for jet formation and that the rate and angular correlation of the jets strongly indicate that the jet events are predominantly produced by resolved processes as required by QCD. The description of the data with the PYTHIA 5.6 jet generator requires a value of $\hat{p}_{T,min}$ of about 2.5 GeV. For this parameter value the jet contribution to the total γp cross section is predicted as $\sigma_{jet} = 30\ \mu b$ in agreement with the assumption made for the total cross section measurement.

SUMMARY

HERA and H1 have appeared on the scene. The main effort at HERA in the near future will be to drastically increase the luminosity which should be possible already this year. Every step in luminosity will give access to new interesting physics. Already the first glimpse to HERA physics gave new physics results.

REFERENCES

1. F. W. Brasse , 'The H1 Detector at HERA ', contribution to this conference
2. W. Buchmüller and G. Ingelmann, Proceedings of the workshop *Physics at HERA* , vol.3, DESY, april 92
3. A.Donnachie and P.V.Landshoff, Nucl.Phys. B231 (1984) 189, H.Abramowicz, E.M.Levin, A.Levy, U.Maor, Phys.Lett. B269 (1991) 465.
4. G.Schuler and J.Terron, CERN-TH 6414/92 (1992), M.Drees and F.Halzen, Phys.Rev.Lett. 61 (1988) 275, R.Gandhi and I.Sarcevic, Phys.Rev. D44 (1991) R10, J.R.Collins and G.A.Ladinsky, Phys.Rev. D43 (1991) 2847.

THE H1 DETECTOR AT HERA

The H1 Collaboration presented by F.W. Brasse
DESY

Abstract

The H1 Detector, built for Physics in e p collisions, is briefly described with its physics potentials. Results on performance are given from measurements on testbeams as well as from first collisions at HERA.

1. GENERAL LAYOUT OF DETECTOR

The Detector is shown in Figure 1 in a vertical cut along the beam, with 30 GeV electrons coming from the left, 820 GeV protons from the right. As the protons have much higher energy than the electrons, the detector is asymmetric with respect to forward and backward direction, defined here in relation to the protons. Starting from the beamline near the interaction point (IP) the detector consists of a central (1) and a forward (2) tracking system. The superconducting coil (6) with a diameter of about 6 m provides a homogeneous longitudinal field of 1.2 T for momentum measurements. For the HERA machine this field is compensated by the superconducting coil (12). A liquid Argon calorimeter consisting of an electromagnetic part (3) built with lead plates and a hadronic part (4) with stainless steel plates is surrounding the trackers guaranteeing a good hermetic coverage in the central and forward region. The coil was placed outside the calorimeter to minimize the material in front of the calorimeter.

The magnetic field is returned by the iron yoke (7). This yoke is laminated and filled with limited streamer tubes to measure the hadronic energy leaking out of the calorimeter and to register muon tracks. These are in addition identified and measured by muon chambers (8) inside and outside the iron. In the forward region a spectrometer with the Toroid (14) and driftchambers (8) provide the measurement of muon tracks.

The calorimetry in the forward region is completed by the plug calorimeter (15) built of copper absorber plates and silicon detector planes. In the backward region the detector is completed by an electromagnetic warm lead scintillator calorimeter (10) with a MWP chamber in front of it to determine the impact point. The TOF time of flight counter system (16) is acting as a veto against p-beam initiated background from upstream.

2. PHYSICS GOALS

The physics goals are summarized in the following list in a sequence of priorities taking into account that the design luminosity of $1.5.10^{31}$ cm^2/sec will only be reached over a length of time with experience for both, the machine and the experiment:

- Low x, low Q^2 deep inelastic scattering to measure e.g. the gluon distribution
- Photoproduction with measurement of σ_{tot}, high P_T and jet production
- Jet physics in deep inelastic scattering with gluon radiation and hard scattering
- Heavy quark production
- Precise measurement of structure functions in NC and CC interactions for test of QCD and determination of parton distributions.
- Measurement of electroweak parameters
- Search for new particles as excited electrons, leptoquarks or heavy neutrinos.

From these goals the requirements for the H1-Detector are:

-Energy calibration for the electromagnetic and hadronic calorimeters of 1-2 %

- Good energy resolution of the electromagnetic calorimeters around $\sigma/E = 10\ \% \sqrt{E}$, possibly even better in the low x (backward) region; moderate energy resolution for hadrons of about 50 - 60 % /$\sqrt{E}$

- Fine granularity of the electromagnetic calorimeter for e/π–separation

- Fine track separation and optimum resolution for charged particles in the trackers

- Some particle identification using dE/dx in the driftchambers and transition radiation in the forward region. Identification of muons over the full acceptance of the detector.

- Tagging of electrons under zero angle in the machine to define the almost real photon for photoproduction.

3. PERFORMANCE OF THE DETECTOR

a) Calorimetry

The liquid **Argon calorimeter** is built in a modular way with 8 rings along the beam direction (Fig. 1), each ring having 8 electromagnetic and 8 hadronic stacks. The sampling cells in the electromagnetic part consist of 2.4 mm thick Pb plates and 2.35 mm Argon gaps with one plane of padreadout boards per gap. The cells in the hadronic part have a total of 19 mm thickness of stainless steel combined with a double gap of 2 x 2.3 mm Argon and a double sided padreadout board. In the forward region for the first four rings and for the eighth ring backward the orientation of the plates is parallel to the beam, in the remaining barrel part it is perpendicular to the beam. Total depths in Xo and λ as well as granularities and numbers of readout cells are given in Table 1. Further details on the construction and readout of the liquid Argon calorimeter can be found elsewhere[1].

To calibrate the stacks and measure resolution at least one stack of each ring has been in a test beam at CERN with electrons and pions in the energy range 5 - 220 GeV. Also combinations of neighboured stacks have been tested to study the effect of cracks with dead material. Results on calibration and resolution are given in Table 1. As the response ratio of electrons and hadrons in Pb and stainless steel is not one, a weighting technique is used to equalize the response[1].

It is important to monitor the calibration during the experiment. This is done with the following methods:

- The Argon purity is constantly checked with several ionization gaps using β-probes, which are distributed over the calorimeter. The stability has been observed to be <0.5 % over one year.

- Electronic calibration with capacitors in the Argon. Stability <0.1 % over periods of months.

- Comparison with momentum of tracks (π, μ, e), measured in the trackers.

Therefore the envisaged calibration of 1-2%, needed for determination of structure function with an error smaller than 10%, can be reached and maintained.

Table 1: Parameters, energy calibration and resolution $\sigma/E=(A^2/E+B^2/E^2+C)^{1/2}$of the calorimeters. *) The range refers to forward - central region. **) Linearity and stability

	Depth Xo/λ	Granularity [cm^2]	# of Channels	Calibration $\Delta E/E$[%]	Energy A[%.GeV$^{1/2}$]	Resolution B [Gev]	C [%]
LAr e$^-$	30-20/1*)	10- 100	30784	$\pm$ 1**)	11.2 $\pm$ .05	.152$\pm$.004	.64$\pm$.07
LAr pion	6- 4 *)	50-2000	13568	$\pm$ 2**)	46.1 $\pm$ .7	. 73$\pm$ .03	2.6 $\pm$ .2
BEMC	22/1	250	88	< $\pm$ 3	10.5	-	-
Tailcatcher	4.5	2500	4000	-	100	-	-
e$^-$Tagger	21	5	49	< $\pm$ 1	12	-	1

The **warm backward calorimeter**, called BEMC, samples with 2.5 mm Pb and 4 mm scintillator and has a readout by silicon diodes via wavelength-shifters placed to the outside of the stacks . With a size of the stacks of 160 x 160 mm^2 a total of 64 quadratic and 24 triangle type stacks cover the backward region with some overlap to the liquid Argon calorimeter.

The energy leaking out of both calorimeters is measured by the streamer tube system, called **tailcatcher**, via pad readout. The system is described in another contribution to this conference[2].

Both, BEMC and tailcatcher, have been measured in test beams. The results are also given in table 1. In addition the present energy calibration of the BEMC has been estimated from e p collisions using the kinematic peak of the scattered electron in deep inelastic scattering at HERA of 26.7 GeV, which is the present primary energy of electrons.

The **plug calorimeter** has the task to check the transverse energy balance in the region of proton fragments. It is however placed behind larger amounts of dead material of beampipe, liquid argon cryostat and forward tracker. The calorimeter is built of 8 75 mm Cu plates with silicon pad readout in the gaps. The granularity of the readout is 50 x 50 mm. Its operation has not yet been explored as it is only partially equipped.

b) Tracking

A detailed view along the beam direction of the central, forward and backward tracking is given in Figure 2. The **MWP chambers**, having pad readout in the central and forward part and wire readout in the backward chamber, are only used for triggering to define either a vertex (central) or a ray (forward). Each of these chambers with pad readout has two planes, the backward chamber has four wire planes rotated by 45° with respect to each other.

The precise determination of tracks in the **central region** is done for the rϕ coordinate by the two jet chambers CJC1 and 2, for the z-coordinate by the two z-chambers CIZ and COZ. Both types of chambers had been experienced in the JADE experiment[3]. The wires are readout at either end to get the coordinate along the wires by charge division. For the jetchamber this information is also used to determine the ionization energy for particle identification. Important parameters of the chambers are given in Fig. 3 and Table 2.

The forward region is equipped with 3 identical supermodules, each one having the series of planar driftchamber, MWPC, transition radiation volume and radial driftchamber. Details about the number of planes and wires per chamber are given in Fig. 4 and some important parameters are in Table 2. As the radial chamber gives only a precise determination of the ϕ coordinate, space points are defined by the planars with different wire orientations. In addition the radial wires are readout at two ends by connecting two wires in different sectors, being 105° apart in ϕ, at the beampipe end.

Table 2: Parameters and track resp. track segment residuals, as determined from first running at HERA, for the driftchambers. All dimensions are in mm.

Chambers	Max.Drift Length	Sense Wire Spacing	# of Sense Wires	$\sigma r\phi$	σz	σr	$\sigma x,y$
Jet	44.5	10.16	2640	0.21	23.5	-	-
Inner z	59.2	7.1	60	25	0.25	-	-
Outer z	44.5	6.0	96	58	0.34	-	-
Forw.Radial	50	10	1728	0.17	-	29	-
Forw.Planar	28	6.0	1152	-	-	-	0.21

The resolutions as given in Table 2 are determined from tracks (jetchambers) resp. track segments as found in real e p data. These resolutions are close to the design values[4].

The resulting momentum resolution in present data using the jetchambers is also not far from the design value, which is $\sigma_p/p^2 \approx 0.3$ % GeV^{-1}.

c) Muon Detection

The chambers inside the gaps of the iron and outside the iron, **the iron instrumentions**, are built of plastic limited streamertube elements. The novel features of these chambers are:

- Halogenfree material (Luranyl instead of PVC)
- Low resistivity coating leading to more stable operation
- Use of nonflammable gas mixture (CO_2/Isobutane/Argon = 88.5/9.5/2.5).

This third point has considerably improved the safety for the whole detector compared to other big experiments.

Detailed information about the system and its performance is given in the report by J.Tutas[2] in these proceedings.

The **forward muon spectrometer** consists of a Toroid with a length of 1.2 m, a field of 1.5 Tesla and a total of 12 driftchamber planes. These planes are arranged as double planes with a shift of the sense wires in one of the planes by half the driftlength with respect to the other one. The drift length is 6 cm. The positions in relation to the toroid are seen in Figure 1. Two of the double planes on either side of the toroid measure the polar angle Θ, the remaining ones the azimuthal angle Φ.

The operation of the Θ chambers has been studied already during the e p collisions. The resolution has been found using halo muons of the proton beam to be $\sigma \leq 0.35$ mm. The momentum resolution is expected to be $\sigma_{p/p} \approx$ 23 - 32 % in the range of 25 - 150 GeV, where it is determined at the lower end by multiple scattering.

d) Luminosity Measurement

The luminosity of electron proton collisions is determined using the Bremsstrahlung process e + p -> e + p + γ by measuring the energy of the electron and the photon. This is done using two calorimeters built of crystals (TlCl/TlBr = 78/22), which are located 34 m (electron) and about 105 m (photon) downstream of the interaction point in the HERA tunnel. The electron calorimeter has a matrix of 7 x 7, the photon calorimeter of 5 x 5 crystals with dimensions of 22 x 22 x 200 mm^3. These crystals have a ratiation length of 9 mm. The energy resolution has been measured in a testbeam to be $\sigma/E = 1\ \% \oplus 12\ \% \sqrt{E}$.

As the electronbeam restgas interaction is also giving Bremsstrahlung a subtraction is made by measuring this component using a noncolliding electron bunch.

The electron calorimeter is also used with an anticoincidence of the photon detector for the measurement of photoproduction using it as a tagger to determine the energy of the almost real photon.

CONCLUSIONS

The H1 detector has been working already for more than one year, starting by measuring cosmic muons in spring 1991. During June/July 1992 first data from electron proton collisions have been taken and analysed and results are presented[5]. During these first runs at HERA the quality and the power of the detector have already been verified.

REFERENCES

1. E. Banas et al., *The H1 Liquid Argon Calorimeter System:* to be submitted to Nucl. Instr. & Math.
2. J. Tutas, *The Limited-Streamer Tube System of H1:* Proceedings of this Conference
3. W. Bartel et al.: Phys. Lett. 88 B (1979), 71
4. H1 Collaboration, *Technical Proposal for the H1 Detector,* 1986
5. F. Eisele, *First results from H1 at HERA:* Proceedings of this Conference.

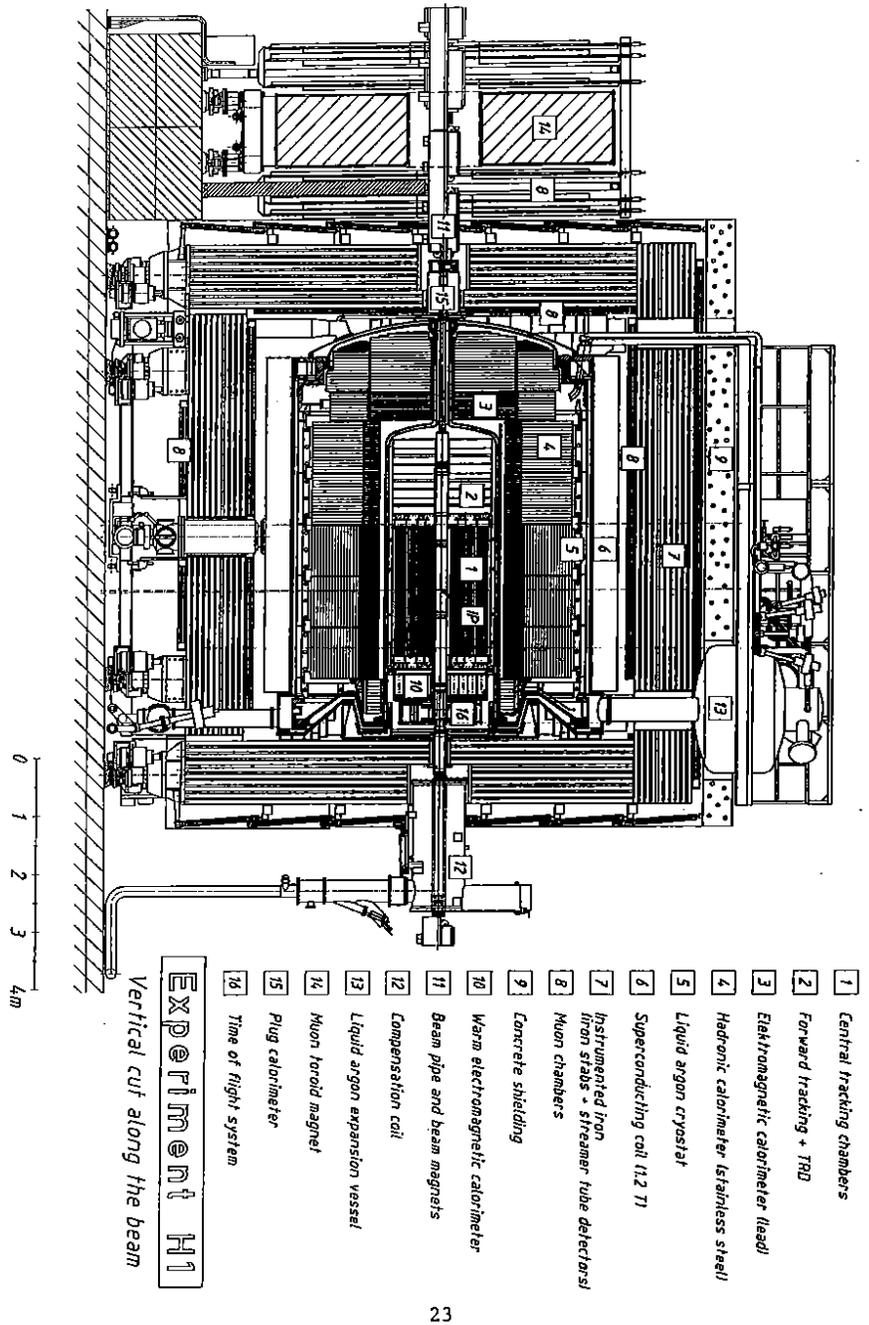

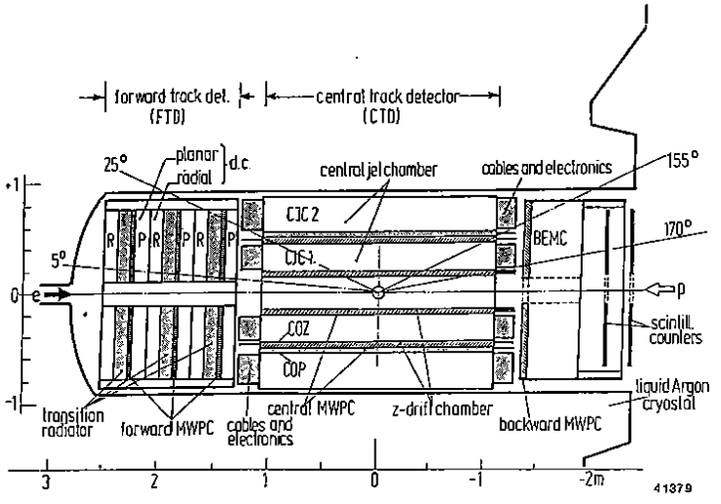

Figure 2. Tracking system, cut along the beam

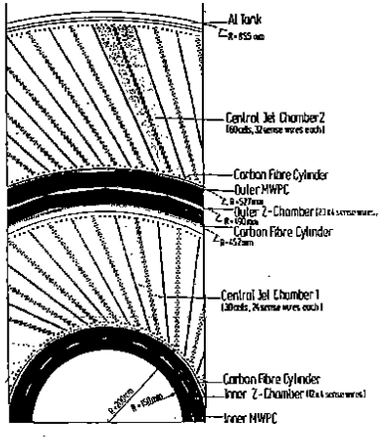

H1 Central Tracking Detectors

Figure 3. Cross sectional view of central trackers

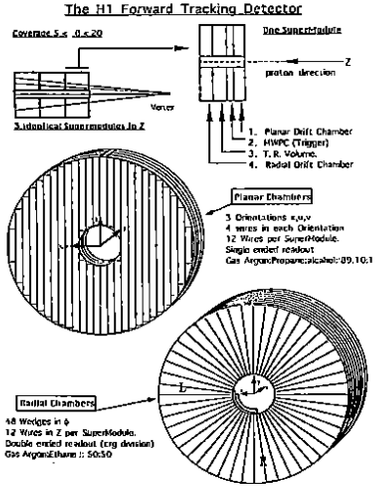

Figure 4. Schematic pictures of forward trackers